J|A|C|S
ARTICLES
Published on Web 12/08/2006

Deviation from the Planarity—a Large Dy_3N Cluster Encapsulated in an I_h-C_{80} Cage: An X-ray Crystallographic and Vibrational Spectroscopic Study

Shangfeng Yang,*,† Sergey I. Troyanov,*,‡ Alexey A. Popov,†,‡ Matthias Krause,†,§ and Lothar Dunsch*,†

Contribution from the Group of Electrochemistry and Conducting Polymers, Leibniz-Institute for Solid State and Materials Research (IFW) Dresden, D-01171 Dresden, Germany, Department of Chemistry, Moscow State University, Leninskie Gory, 119992 Moscow, Russia, and Institute of Ion Beam Physics and Materials Research, Forschungszentrum Rossendorf, PF 510119, D-01314 Dresden, Germany

Received September 21, 2006; E-mail: s.yang@ifw-dresden.de; stroyano@thermo.chem.msu.ru; l.dunsch@ifw-dresden.de

Abstract: The high-yield synthesis of $Dy_3N@C_{80}$ (I) opens the possibility of characterizing its molecular and vibrational structures. We report on the structure determination of $Dy_3N@C_{80}$ (I) by X-ray crystallographic study of single crystal of $Dy_3N@C_{80}$·Ni(OEP)·$2C_6H_6$, revealing a nearly planar Dy_3N cluster encapsulated in an I_h-C_{80} cage. The vibrational structure of $Dy_3N@C_{80}$ (I) is studied by Fourier transform infrared (FTIR) and Raman spectroscopy in combination with force-field calculations. A correlation was found between the antisymmetric metal-nitrogen stretching vibration and the structure of the M_3N cluster of $M_3N@C_{80}$ (I) (M = Y, Gd, Tb, Dy, Ho, Er, Tm). Moreover, a stronger interaction between the encaged nitride cluster and the C_{80} carbon cage was found in the class II $M_3N@C_{80}$ (I) (M = Y, Gd, Tb, Dy, Ho, Er, Tm) than in $Sc_3N@C_{80}$ (I). This study demonstrates that the cluster size plays the dominating role in the structure of the M_3N cluster in $M_3N@C_{80}$ (I).

Introduction

Because of the feasibility of tuning the trapped metal atoms and of stabilizing a large variety of cage sizes including different isomeric structures, trimetallic nitride endohedral fullerenes (clusterfullerenes),[1−2] a new class of fullerenes with a trimetallic nitride cluster encaged, have been attracting great interest since their discovery in 1999.[1−7] As the first member of this new family, $Sc_3N@C_{80}$ (I) can be formally viewed as a positively charged planar cluster of Sc_3N inside a negatively charged icosahedral (I_h) carbon cage, that is, $[Sc_3N]^{6+}@C_{80}^{6-}$.[3,8] Later on, within several other Sc-based clusterfullerenes such as $Sc_3N@C_{80}$ (II),[7a,9] $Sc_3N@C_{78}$,[7e,10] and $Sc_3N@C_{68}$,[6d,11,12] the Sc_3N cluster was revealed to remain planar. Furthermore, other clusters including $ErSc_2N$, $CeSc_2N$, Lu_3N, and Tb_3N were found to be also planar in $ErSc_2N@C_{80}$,[13] $CeSc_2N@C_{80}$,[14] $Lu_3N@C_{80}$,[15a] and $Tb_3N@C_{84}$,[15b] respectively. An intriguing exception reported to date was found in $Gd_3N@C_{80}$ (I), for which the Gd_3N was pyramidal with the N atom displacing ca. 0.5 Å out of the Gd plane as reported on the basis of X-ray crystallographic data.[16] The differences in the pyramidalization of the N atom in these

† Leibniz-Institute for Solid State and Materials Research.
‡ Moscow State University.
§ Institute of Ion Beam Physics and Materials Research.

(1) Dunsch, L.; Krause, M.; Noack, J.; Georgi, P. *J. Phys. Chem. Solids* **2004**, *65*, 309−315.
(2) For recent invited review, see (a) Dunsch, L.; Yang, S. *Small*, submitted. (b) Dunsch, L.; Yang, S. *Electrochem. Soc. Interface* **2006**, *15* (2), 34−39.
(3) Stevenson, S.; Rice, G.; Glass, T.; Harich, K.; Cromer, F.; Jordan, M. R.; Craft, J.; Hajdu, E.; Bible, R.; Olmstead, M. M.; Maitra, K.; Fisher, A. J.; Balch, A. L.; Dorn, H. C. *Nature* **1999**, *401*, 55−57.
(4) Dunsch, L.; Georgi, P.; Krause, M.; Wang, C. R. *Synth. Met.* **2003**, *135*, 761−762.
(5) Dunsch, L.; Georgi, P.; Ziegs, F.; Zöller, H. German Patent DE 10301722 A1, 2003.
(6) (a) Yang, S.; Dunsch, L. *J. Phys. Chem. B* **2005**, *109*, 12320−12328. (b) Yang, S.; Dunsch, L. *Angew. Chem., Int. Ed.* **2006**, *45*, 1299−1302. (c) Yang, S.; Dunsch, L. *Chem. Eur. J.* **2006**, *12*, 413−419. (d) Yang, S.; Kalbac, M.; Popov, A.; Dunsch, L. *Chem. Eur. J.* **2006**, *12*, 7856−7863. (e) Yang, S.; Kalbac, M.; Popov, A.; Dunsch, L. *ChemPhysChem.* **2006**, *7*, 1990−1995.
(7) (a) Krause, M.; Dunsch, L. *ChemPhysChem.* **2004**, *5*, 1445−1449. (b) Krause, M.; Wong, J.; Dunsch, L. *Chem. Eur. J.* **2005**, *11*, 706−711. (c) Krause, M.; Dunsch, L. *Angew. Chem., Int. Ed.* **2005**, *44*, 1557−1560. (d) Krause, M.; Liu, X.; Wong, J.; Pichler, T.; Knupfer, M.; Dunsch, L. *J. Phys. Chem. A* **2005**, *109*, 7088−7093. (e) Krause, M.; Popov, A.; Dunsch, L. *ChemPhysChem.* **2006**, *7*, 1734−1740.
(8) Alvarez, L.; Pichler, T.; Georgi, P.; Schwieger, T.; Peisert, H.; Dunsch, L.; Hu, Z.; Knupfer, M.; Fink, J.; Bressler, P.; Mast, M.; Golden, M. S. *Phys. Rev. B* **2002**, *66*, 035107-1-7.
(9) Cai, T.; Xu, L. S.; Anderson, M. R.; Ge, Z. X.; Zuo, T. M.; Wang, X. L.; Olmstead, M. M.; Balch, A. L.; Gibson, H. W.; Dorn, H. C. *J. Am. Chem. Soc.* **2006**, *128*, 8581−8589.
(10) Olmstead, M. M.; Bettencourt-Dias, A.; Duchamp, J. C.; Stevenson, S.; Marciu, D.; Dorn, H. C.; Balch, A. L. *Angew. Chem., Int. Ed.* **2001**, *40*, 1223−1225.
(11) Stevenson, S.; Fowler, P. W.; Heine, T.; Duchamp, J. C.; Rice, G.; Glass, T.; Harich, K.; Hajdu, E.; Bible, R.; Dorn, H. C. *Nature* **2000**, *408*, 427−428.
(12) Olmstead, M. M.; Lee, H. M.; Duchamp, J. C.; Stevenson, S.; Marciu, D.; Dorn, H. C.; Balch, A. L. *Angew. Chem., Int. Ed.* **2003**, *42*, 900−903.
(13) Olmstead, M. M.: de Bettencourt-Dias, A.; Duchamp, J. C.; Stevenson, S.; Dorn, H. C.; Balch, A. L. *J. Am. Chem. Soc.* **2000**, *122*, 12220−12226.
(14) Wang, X. L.; Zuo, T. M.; Olmstead, M. M.; Duchamp, J. C.; Glass, T. E.; Cromer, F.; Balch, A. L.; Dorn, H. C. *J. Am. Chem. Soc.* **2006**, *128*, 8884−8889.
(15) (a) Stevenson, S.; Lee, H. M.; Olmstead, M. M.; Kozikowski, C.; Stevenson, P.; Balch, A. L. *Chem. Eur. J.* **2002**, *8*, 4528−4535. (b) Beavers, C. M.; Zuo, T.; Duchamp, J. C.; Harich, K.; Dorn, H. C.; Olmstead, M. M.; Balch, A. L. *J. Am. Chem. Soc.* **2006**, *128*, 11352−11353.
(16) Stevensen, S.; Phillips, J. P.; Reid, J. E.; Olmstead, M. M.; Rath, S. P.; Balch, A. L. *Chem. Commun.* **2004**, 2814−2815.

clusterfullerenes were interpreted by the discrepancy in the ionic radius of the metals encaged.[16] In fact, Gd_3N is the largest cluster encaged in fullerene cages so far.[7c] This results in another remarkable uniqueness of $Gd_3N@C_{80}$ in terms of its much lower yields and the smaller cage size distribution of $Gd_3N@C_{2n}$ clusterfullerenes ($40 \leq n \leq 44$) compared to those clusterfullerenes encaging other metals with smaller ionic radius such as Tm.[7b,c] Likewise, the same pyramidal cluster structure was also proposed very recently for Gd_2ScN in $Gd_2ScN@C_{80}$ (I) by our group.[6e] Moreover, the Y_3N unit in a pyrrolidine adduct of $Y_3N@C_{80}$ was revealed by X-ray crystallographic data to be slightly pyramidalized with the N atom displacing only 0.13 Å out of the Y_3 plane in a more recent report.[17]

We have recently isolated dysprosium-based nitride clusterfullerenes by the ''reactive gas atmosphere" method.[6a] The dysprosium (Dy) has a relatively large ionic radius (Dy^{3+}, 0.91 Å) which is close to those of Gd^{3+} (0.94 Å) and Y^{3+} (0.90 Å) but significantly larger than those of Sc^{3+} (0.75 Å) and Lu^{3+} (0.85 Å).[18] With such an intermediate ionic radius of Dy^{3+}, an important question to be addressed is which structure the Dy_3N cluster would take within $Dy_3N@C_{80}$ (I).

In this paper, we report on the structure determination of $Dy_3N@C_{80}$ (I) by X-ray crystallographic study. The structural data are correlated with the Fourier transform infrared (FTIR) and Raman spectroscopic characterization, which provides detailed insight into the vibrational structure of $Dy_3N@C_{80}$ (I), the dependence of the cluster structure on the ionic radius of the metal encaged, and the interaction between the nitride cluster and the C_{80} cage.

Experimental Section

General procedures for the synthesis of $Dy_3N@C_{80}$ (I) clusterfullerenes by a modified Krätschmer-Huffman DC-arc discharging method with the addition of NH_3 (20 mbar) have been described elsewhere.[1,2,4−7] After DC-arc discharging, the soot was pre-extracted by using acetone and was further Soxhlet-extracted by CS_2 for 20 h. Clusterfullerene separation from empty fullerenes was performed by single-stage high-performance liquid chromatography (HPLC) running in a Hewlett-Packard instrument (series 1050), with toluene used as the eluent (mobile phase) at the flow rate of 1.6 mL/min. A linear combination of two analytical 4.6 × 250 mm Buckyprep columns (Nacalai Tesque, Japan) was applied to separate $Dy_3N@C_{80}$ (I). A UV detector set to 320 nm was used for fullerene detection. The purity of the isolated product was further checked by HPLC runs performed on a 10 × 250 mm Buckyclutcher column (Regis, United States), followed by Laser-desorption Time-of-flight (LD-TOF) mass spectrometric (MS) analysis running in both positive and negative ion modes (Biflex III, Bruker, Germany).

Crystal growth for $Dy_3N@C_{80}$·Ni(OEP)·$2C_6H_6$ was accomplished by layering a solution of ca. 1.0 mg $Dy_3N@C_{80}$ (I) in 1 mL benzene over a solution of 3.0 mg Ni^{II}(OEP) in 3 mL benzene. After the two solutions diffused together over a period of 7 days, small black crystals suitable for X-ray crystallographic study formed upon a slow evaporation of benzene. X-ray data collection for the crystal of $Dy_3N@C_{80}$·Ni(OEP)·$2C_6H_6$ ($0.03 \times 0.02 \times 0.02$ mm^3) was carried out at 100 K at the Protein Structure Factory beamline BL14.2 of BESSY (Free University Berlin at BESSY, Berlin, Germany) with an MAR345 image plate detector. $Dy_3N@C_{80}$·Ni(OEP)·$2C_6H_6$ crystallizes in the monoclinic space group $C2/c$; $a = 25.3119(2)$ Å, $b = 15.0979(1)$ Å, $c = 39.4098(3)$ Å, $V = 14998.9(2)$ Å^3, $Z = 8$. 54 495 reflections collected; 13 352 reflections independent; no absorption correction was performed. The structure was solved using direct methods (SHELXS97).[19] Full-matrix least-squares anisotropic refinement (SHELXL97) was carried out for all non-hydrogen atoms (most H's were included in calculated positions) with 13 337 reflections and 1288 parameters converged to $wR_2 = 0.2383$ and $R_1 = 0.0864$ for 11 051 reflections with $I > 2\sigma(I)$. The Dy_3N unit was found to be disordered between three positions with occupancy factors of 0.662, 0.303, and 0.035. The C_{80} cage is ordered, but some carbon atoms have unreliable anisotropic displacement parameters, most obviously because of the disorder of the Dy_3N unit in the cage. One benzene molecule is also disordered. CCDC 621034 contains the supplementary crystallographic data for this paper. These data can be obtained free of charge on application to the Cambridge Crystallographic Data Center, 12 Union Road, Cambridge CB2 1EZ, United Kingdom (fax: (+44) 1223-336-033; e-mail: deposit@ccdc.cam.ac.uk).

For FTIR and Raman measurements, approximately 100 μg $Dy_3N@C_{80}$ (I) was drop-coated on KBr single-crystal disks. The residual toluene was removed by heating the polycrystalline films in a vacuum of 2×10^{-6} mbar at 235 °C for 3 h. The FTIR spectra were recorded at room temperature in transmission mode by an IFS 66v spectrometer (Bruker, Germany) with a resolution of 2 cm^{-1}. Raman scattering was excited by the 647- and 514-nm emission lines of a Kr^+ ion and an Ar^+ ion laser, respectively (Innova 300 series, Coherent, United States). The scattered light was collected in a 180° backscattering geometry and was analyzed by a T 64000 triple spectrometer (Jobin-Yvon, France) whose spectral band-pass was set to 2 cm^{-1}. A rotation device was used as sample holder to exclude heat-induced sample changes in the Raman experiments.

Density Functional Theory (DFT) computations were performed with the use of PRIRODA package employing PBE density functional and implemented TZ2P-quality basis set with effective-core potential for metal atoms.[6d,6e,7e]

Results and Discussion

Synthesis and Isolation of $Dy_3N@C_{80}$ (I). The high-yield synthesis of $Dy_3N@C_{80}$ (I) clusterfullerene by the reactive gas atmosphere method[1,2,4−7] is demonstrated in Figure 1a, which represents a typical chromatogram of a $Dy_3N@C_{2n}$ fullerene extract mixture. In combination with the mass spectroscopic (MS) analysis, the abundance of $Dy_3N@C_{2n}$ ($39 \leq n \leq 44$) clusterfullerenes as the main products reaches up to 98% of all of the fullerenes, overwhelmingly higher than those of the empty fullerenes (~2%).[6a] Among them, the most abundant product is $Dy_3N@C_{80}$ (I) (fraction A, $t_{ret} = 33.4$ min), whose relative yield reaches up to 65−70% of all of the fullerenes. On the other hand, the abundance of $Dy_3N@C_{80}$ (I) is approximately 25-fold higher than that of C_{60} ($t_{ret} = 9.6$ min) as estimated from the integrated peak area.[6c] The reason for such an exceptional high yield has been proposed previously.[6a]

Facilitated by such a high-yield synthesis, $Dy_3N@C_{80}$ (I) is readily isolated by single-step HPLC to high purity (≥99%), which is ascertained by the further HPLC analysis and laser desorption time-of-flight (LD-TOF) MS analysis (Figure 1b). A closer comparison of the measured isotope distribution for the $Dy_3N@C_{80}$ (I) ($m/z = 1462$) with the theoretical calculation indicates fairly good agreement as demonstrated in Figure 1b, confirming the proposed chemical form. Such a high purity provides the prerequisite for the following X-ray crystallographic and spectroscopic characterization.

(17) Echegoyen, L.; Chancellor, C. J.; Cardona, M. M.; Elliott, B.; Rivera, J.; Olmstead M. M.; Balch, A. L. *Chem. Commun.* **2006**, 2653−2656.
(18) Greenwood, N. N.; Earnshaw, A. *Chemistry of the Elements*; Pergamon: Oxford, U.K., 1984.
(19) (a) Sheldrich, G. M. *Acta Crystallogr., A* **1990**, *46*, 467. (b) Troyanov, S. I.; Popov, A. A. *Angew. Chem., Int. Ed.* **2005**, *44*, 4215−4218.

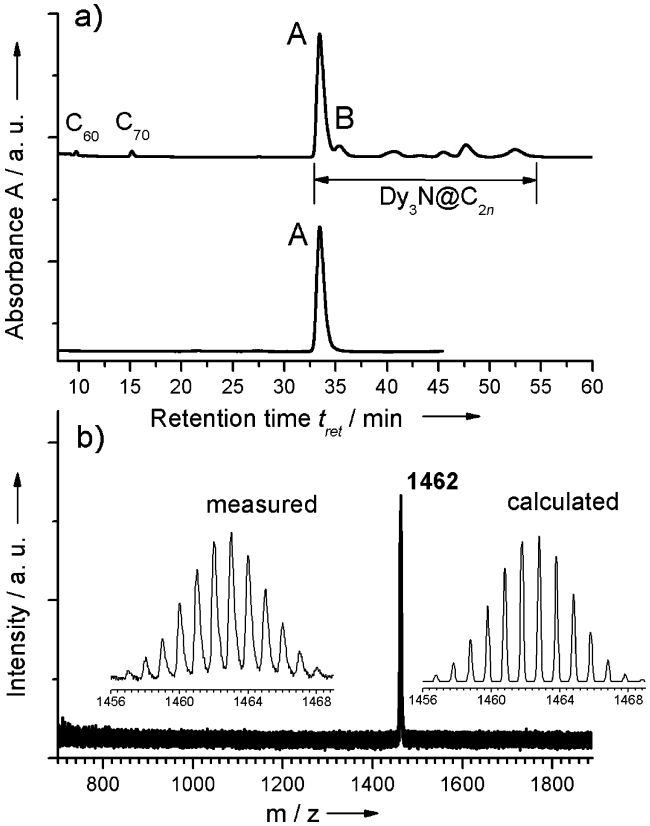

Figure 1. (a) Chromatograms of a $Dy_3N@C_{2n}$ fullerene extract mixture (upper trace) and the isolated $Dy_3N@C_{80}$ (I) (lower trace) (linear combination of two 4.6 × 250 mm Buckyprep columns; flow rate 1.6 mL/min; injection volume 100 μL; toluene as eluent (mobile phase); 40 °C). The peaks with t_{ret} = 32.7∼54.7 min correspond to $Dy_3N@C_{2n}$ ($39 \le n \le 44$) clusterfullerenes. A: $Dy_3N@C_{80}$ (I); B: $Dy_3N@C_{80}$ (II). (b) Positive ion LD-TOF mass spectrum of the isolated $Dy_3N@C_{80}$ (I). The insets show the measured and calculated isotope distributions of $Dy_3N@C_{80}$ (I).

Structure Determination of $Dy_3N@C_{80}$ (I) by X-ray Crystallography. By cocrystallization with $M^{II}(OEP)$ ($M^{II}C_{36}H_{44}N_4$, M = Ni, Co; OEP = dianion of octaethylporphyrin), endohedral fullerenes have been found to crystallize in an ordered manner.[3,10−16] $Dy_3N@C_{80}$ (the label of isomer I is omitted below for clarification) was successfully cocrystallized with Ni(OEP), resulting in the black crystals of $Dy_3N@C_{80}$·Ni(OEP)·$2C_6H_6$. Figure 2 shows its X-ray structure, indicating clearly the relative orientations of $Dy_3N@C_{80}$ and Ni(OEP). As convinced by an R_1 of 0.086 which is superior compared to some values of the other reported endohedral fullerene structures,[3,10,12,13] a good quality of the $Dy_3N@C_{80}$·Ni(OEP)·$2C_6H_6$ crystal ensures the following structure elucidation. A noteworthy feature found for the $Dy_3N@C_{80}$·Ni(OEP)·$2C_6H_6$ crystal is a doubling of the unit cell parameter *c* (39.4 Å) as compared with the values for analogous compounds on the basis of other clusters such as Gd_3N, Sc_3N.[3,16] The space group *C*2/*c* (instead of *C*2/*m*) does not contain a mirror plane, the symmetry element which is responsible for the disorder of the C_{80} fullerene cage (unavoidably resulting in some uncertainty in the crystal structure), therefore, in the $Dy_3N@C_{80}$·Ni(OEP)·$2C_6H_6$ crystal, the I_h-C_{80} cage was found to be ordered in contrast to the other reported cases of $M_3N@C_{80}$·Ni(OEP) complexes.[3,16,20] The factors

(20) The determined space group of *C*2/*c* for $Dy_3N@C_{80}$·Ni(OEP)·$2C_6H_6$, which is different from those of the analogous compounds (*C*2/*m*) for $M_3N@C_{80}$ (I) (M = Sc, Gd, refs 3 and16), and the doubling of the *c* parameter indicate that the reason of a mirror disorder of the C_{80} cage reported in refs 3 and 16 was simply a nonperfect crystallization. This resulted in an irregular translation along the *c* axis and, consequently, in averaging of two mirrored orientations of the C_{80} cage, whereas the M(OEP) units (oriented more symmetrically relative the crystallographic axes) appeared to be not disordered. However, in a more recent report on $CeSc_2N@C_{80}$ (ref 14), the determined space group (*C*2/*c*) and *c* parameter were almost identical to our case, confirming the more perfect crystallization for $Dy_3N@C_{80}$·Ni(OEP)·$2C_6H_6$ as well as $CeSc_2N@C_{80}$ reported in ref 14, resulting in the more ordered I_h-C_{80} cage for both cases.

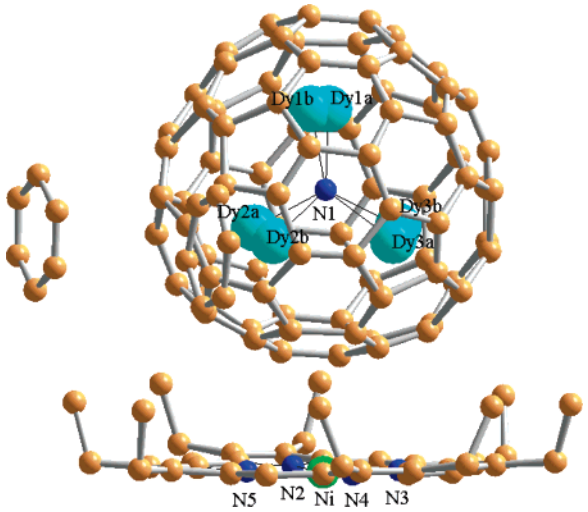

Figure 2. A perspective view of the relative orientations of $Dy_3N@C_{80}$ and Ni(OEP) within the $Dy_3N@C_{80}$·Ni(OEP)·$2C_6H_6$ crystal. Only one benzene molecule is shown for clarity.

responsible for these differences could be, for example, a high purity of $Dy_3N@C_{80}$, which is free of the contamination of any other isomers as discussed above, or some peculiarities of the crystal growth methods used.

Although the C_{80} cage is ordered, the encaged Dy_3N cluster was found to be slightly disordered with two main positions within the C_{80} cage as illustrated in Figure 3. As a matter of fact, endohedral fullerenes cocrystallized with metalloporphyrins generally exhibit some degree of disorder in either the cage orientation, in the location of the metal ions inside the cage, or both.[3,10−16] The positions of Gd atoms within $Gd_3N@C_{80}$ (I) were found to be severely disordered,[16] while in a more recent study, the $CeSc_2N$ unit within $CeSc_2N@C_{80}$ was claimed to be fully ordered.[14] In this sense, it seems that the ordering state of the encaged cluster is strongly dependent on the metal ions. For the case of $Dy_3N@C_{80}$·Ni(OEP)·$2C_6H_6$ crystal, there are primarily two positions of Dy atoms as denoted by "a" and "b" in Figure 3a. The relative occupancies of the positions of "a" and "b" are in a ratio of ca. 2:1. Besides, there is an additional position of Dy1c (not shown) with a contribution of only 3.5%. Consequently, the position of the N atom in the center of the cluster can be split in principle. However, the N atom could be refined as a single atom, that is, with a common position for two Dy_3 triangles. Its thermal ellipsoid is strongly elongated approximately perpendicular to the Dy triangles planes, thus reflecting most probably a real vibrational displacement in this direction. The center of the N ellipsoid lies virtually in both Dy_3 planes (with deviations of only 0.06−0.08 Å), that is, the Dy_3N unit can be regarded as nearly planar (see Figure 4). Within the Dy_3N unit, the Dy−Dy distances in the two main triangles are in the range of 3.45−3.56 Å and Dy−N distances span the range of 2.00−2.07 Å.

Also shown in Figure 3 are the possible interactions of the Dy atoms with the C atoms of the C_{80} cage. It is found that the

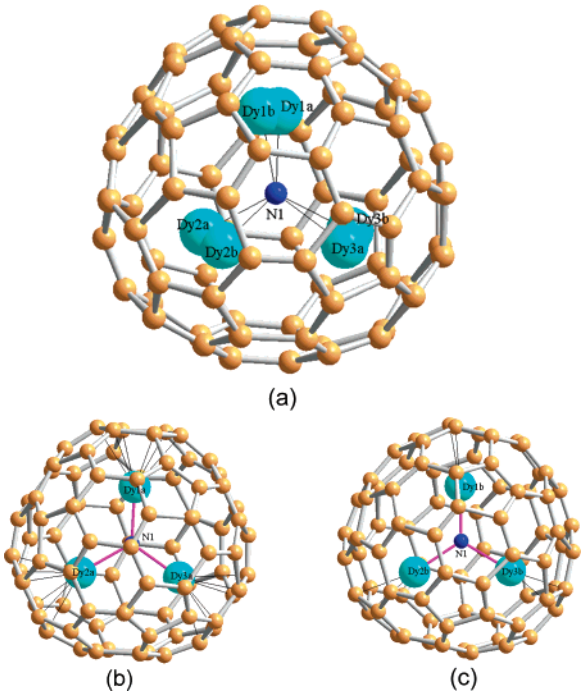

Figure 3. (a) Two positions of Dy3 units (atoms) within the $Dy_3N@C_{80}$·Ni(OEP)·$2C_6H_6$ crystal. The cage with Dy1a−3a (nearly along the C_3 axis) is shown in (b) with the thin lines demonstrating possible interactions of Dy3 atoms with the cage while in (c) only two shortest distances are shown for Dy1b-3b.

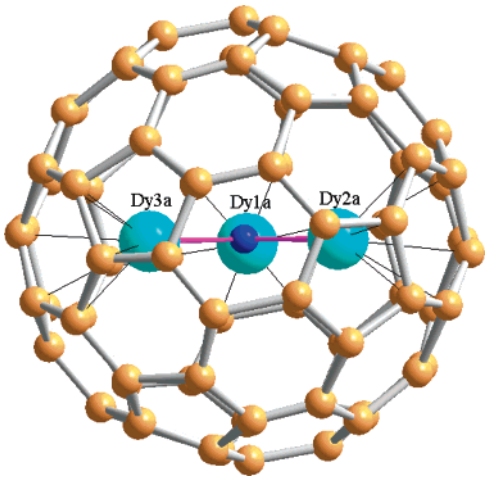

Figure 4. The side view of $Dy_3N@C_{80}$ showing the nearly planar arrangement of the Dy_3 atoms (position "a").

Dy atoms in the main orientation of the Dy_3N unit ("a") coordinate with the six carbon atoms of the hexagons, and the Dy−C distances lie in the range of 2.37−2.46 Å (Figure 3b).[21] This means that the positions of Dy1a−Dy3a atoms in the C_{80} cage (against three coordinated hexagons) are displaced at ca. 120° relative to each other, that is, $Dy_3N@C_{80}$ unit exhibits an approximate C_3 symmetry in this main orientation ("a") and the Dy_3N cluster is nearly planar as shown in Figure 4. However, the interactions of the Dy1b−Dy3b atoms seem to be somewhat different, resulting in a coupling to different sites of the C_{80} cage, where the centering is not as regular as that for Dy1a−Dy3a (Figure 3c). Instead, Dy1b−Dy3b atoms tend to be directed to the C−C bonds (the 6:5 ring junctions).[22]

(21) Dy-to-ring center distances are 1.941, 1.927, and 1.936 Å, smaller than those for the case of Gd3 reported in ref 16.

In terms of the planarity of the M_3N cluster, $Dy_3N@C_{80}$ appears to resemble $Sc_3N@C_{80}$ (I) more than $Gd_3N@C_{80}$ (I) in which the Gd_3N unit was pyramidal.[3,16] In fact, although the ionic radius of Dy^{3+} (0.91 Å) is only slightly smaller than that of Gd^{3+} (0.94 Å),[18] $Dy_3N@C_{80}$ has a much higher yield than $Gd_3N@C_{80}$ (I) and $Dy_3N@C_{2n}$ clusterfullerenes have a much larger cage size distribution than $Gd_3N@C_{2n}$ as demonstrated previously.[6a,7c] On the other hand, regardless of the fact that the ionic radius of Dy^{3+} is significantly larger than that of Sc^{3+} (0.75 Å),[18] it has been previously demonstrated that $Dy_3N@C_{2n}$ clusterfullerenes seem to have a reasonable similarity to $Sc_3N@C_{2n}$ in terms of the yield.[6a,7a] Both the present X-ray crystallographic results and the chromatographic results discussed above reveal that, in addition to the demonstrated influence of the cluster size (ionic radius of the metal) on the cage size distribution and abundance of the clusterfullerenes, the cluster size plays the dominating role in the structure of the encaged M_3N cluster, as described further below.

Structure of $M_3N@C_{80}$ Studied by FTIR Spectroscopy. Infrared spectroscopy has been demonstrated by our group to be a powerful tool for the structural analysis of fullerenes.[1,2,4−7] Figure 5 compares the FTIR spectra of $Dy_3N@C_{80}$ and its counterparts $M_3N@C_{80}$ (I) (M = Sc, Gd, Tb, Ho, Er, Tm, Y) (curves b−g).[1,2,6c,7a−c] A small number of lines are observed for each fullerene. As we have established in our previous work, the region of 1100−1600 cm^{-1} is featured by the tangential C_{80} modes and the band around 500 cm^{-1} is correlated with the IR-active radial cage mode of $M_3N@C_{80}$ (I).[1,2,4−7,23,24] The spectral pattern of $Dy_3N@C_{80}$ is almost identical with those of the other reported $M_3N@C_{80}$ (I) (M = Y, Gd, Tb, Ho, Er, Tm) and is slightly different from the spectrum of $Sc_3N@C_{80}$ (I).[1,2,6c,7a−c,23,24] It has been shown that the clusterfullerenes $M_3N@C_{80}$ (I), despite their identical cage symmetry of I_h,[1,2,6c,7a−c,23,24] can be classified into two classes on the basis of the tangential cage modes, corresponding bond orders, and the electronic properties.[7d] Class I $M_3N@C_{80}$ (I) up to now includes only $Sc_3N@C_{80}$ (I), whose tangential mode frequencies are 4−8 cm^{-1} higher than those of class II clusterfullerenes $M_3N@C_{80}$ (M = Y, Gd, Tb, Ho, Er, Tm). Since the tangential modes of $Dy_3N@C_{80}$ exhibit downshifts of exactly 4−8 cm^{-1} compared to $Sc_3N@C_{80}$ (I), $Dy_3N@C_{80}$ is classified as class II clusterfullerene as well (see Supporting Information S1).

According to our previous work,[1,2,6c,7a−c,21,22] the strongest low-energy IR lines of $Dy_3N@C_{80}$ at 701 and 711 cm^{-1} (see Figure 5) can be unambiguously assigned to the antisymmetric Dy−N stretching vibrations. In fact, such an assignment is commonly established for all reported clusterfullerenes $M_3N@C_{80}$ (I), which generally exhibit the metal-dependent antisymmetric M−N stretching vibration in the region of 600−800 cm^{-1}.[1,2,6c,7a−c,23,24] The antisymmetric M−N stretching vibrations of all $M_3N@C_{80}$ (I) (M = Sc, Y, Gd, Tb, Dy, Ho, Er, Tm) are summarized in Table 1.[7a,7c] The antisymmetric M−N stretching vibrations of $Dy_3N@C_{80}$ have nearly identical frequencies as those of $M_3N@C_{80}$ (I) (M = Ho, Er, Tm) (see

(22) Because the carbon cage atoms involved in interactions with Dy atoms are somewhat pushed outward from the cage, there is an additional small disorder for these atoms (because of the disorder of Dy atoms), thus explaining some irregularities (or distortions) for thermal ellipsoids of a few carbon atoms of the C_{80} cage.

(23) Krause, M.; Kuzmany, H.; Georgi, P.; Dunsch, L.; Vietze, K.; Seifert, G. *J. Chem. Phys.* **2001**, *115*, 6596−6605.
(24) Akasaka, T.; Nagase S. *Endofullerenes: A New Family of Carbon Cluster*; Kluwer Academic Publishers: Dordrecht, 2002.

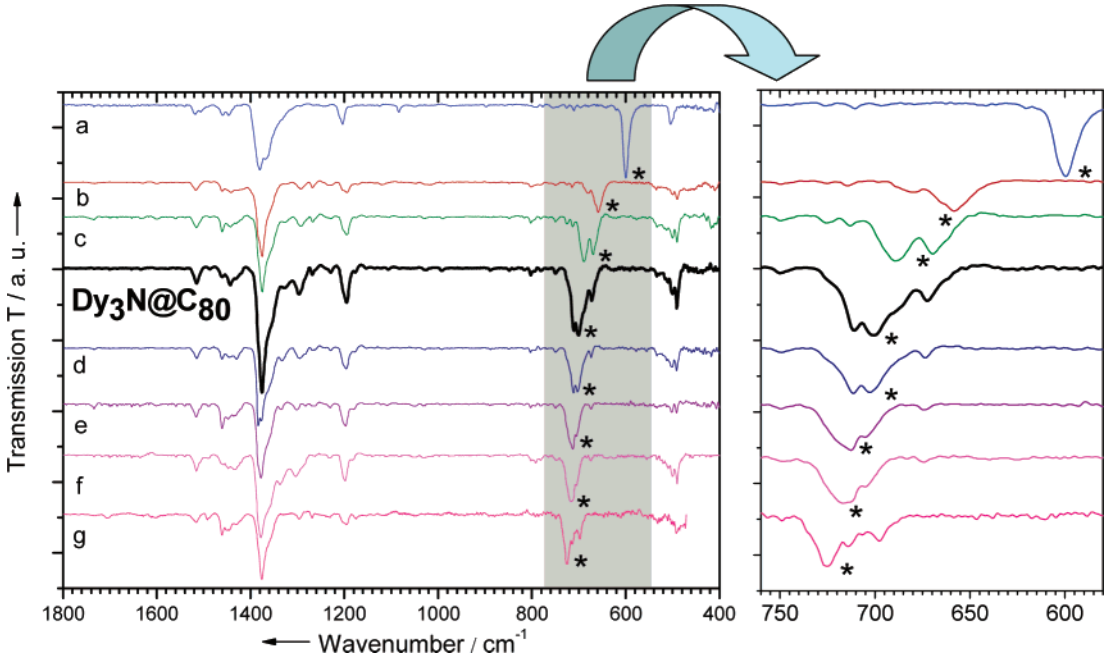

Figure 5. FTIR spectrum of $Dy_3N@C_{80}$ (I) in comparison with other $M_3N@C_{80}$ (I) clusterfullerenes (500 accumulations, 2 cm^{-1} resolution). M = Sc (a), Gd (b), Tb (c), Ho (d), Er (e), Tm (f), Y (g). The asterisks mark the antisymmetric M−N stretching vibrational modes.

Table 1. Characteristic Parameter of $M_3N@C_{80}$ (I) and Structure of the Encaged M_3N Cluster[f]

M	$r(M^{3+})$ (Å)	expt $\nu_{as,M-N}$ (cm^{-1})	expt $\nu_{def,M3N}$ (cm^{-1})	calcd $\nu_{def,M3N}$[a] (cm^{-1})	calcd $\nu_{def,M3N}$[b] (cm^{-1})	structure of cluster	reference
La	1.05					pyramidal[c]	26
Gd	0.94	657	165	140.6	159.6	pyramidal	16
Tb	0.92	669, 689	163	140.1	159.1	pyramidal[d]	
Dy	0.91	701, 711	163	138.9	157.9	nearly planar	this work
Ho	0.90	703, 711	160	138.2	157.2	planar[d]	
Er	0.88	704, 713	158.5	137.5	156.5	planar[d]	13[e]
Tm	0.87	710	157	137.0	156.0	planar[d]	
Lu	0.85			135.3	154.2	planar	15a
Y	0.90	712, 724, 733	194	171.2	189.6	slightly pyramidal	17
Sc	0.75	599	210	203.0	216.6	planar	3

[a] Calculated with the use of $Sc_3N@C_{80}$ (I) force field. [b] Calculated with the use of $Y_3N@C_{80}$ (I) force field. [c] Not isolated experimentally. Predicted by theoretical computations in ref 26. [d] Predicted by this study. [e] Only $ErSc_2N$ unit was reported to be planar within $ErSc_2N@C_{80}$ (I) in ref 13. [f] $r(M^{3+})$: ionic radius of M^{3+}; $\nu_{as,M-N}$: M−N antisymmetric stretching vibrational frequencies;[1,7d] $\nu_{def,M3N}$: in-plane M_3N cluster deformation mode.[7d]

Table 1).[1,7b] However, the Gd−N stretching frequency (657 cm^{-1}) is dramatically smaller, which could be understood by the reduced effective Gd−N force constant because of the pyramidal structure of Gd_3N cluster.[6e,16] This suggests that the M−N stretching frequency is correlated with the structure of M_3N, which is strongly dependent on the cluster size (ionic radius of the metal) as discussed above. Accordingly, it is reasonable to address the structures of the other M_3N clusters in $M_3N@C_{80}$ (I) (M = Tb, Ho, Er, Tm), for which the X-ray crystallographic study has not been reported up to date, on the basis of the analysis of their antisymmetric M−N vibrational frequencies. The Tb−N stretching frequency of $Tb_3N@C_{80}$ (669, 689 cm^{-1}) is closer to ν_{as}(Gd−N) in $Gd_3N@C_{80}$ than to ν_{as}(Dy−N) in $Dy_3N@C_{80}$ (see Table 1). Since lowering of ν_{as}(M−N) is the result of the decrease of force constant caused by pyramidalization, a pyramidal structure is predicted for the Tb_3N cluster within $Tb_3N@C_{80}$ (I). The pyramidal Tb_3N structure can be rationalized by the intermediate ionic radius of Tb^{3+} (0.92 Å) compared to Gd^{3+} (0.94 Å) and Dy^{3+} (0.91 Å),[18] which gives an intermediate size of Tb_3N between Gd_3N and Dy_3N. Contrarily, with a relatively smaller cluster size than in Dy_3N and comparable M−N stretching frequencies, the Ho_3N, Er_3N, and Tm_3N clusters are expected to be rigorously or nearly planar within the corresponding $M_3N@C_{80}$ (I) clusterfullerenes (see Table 1). In this sense, Dy_3N is believed to be the largest uniform lanthanide metal cluster which adopts a nearly planar structure within the I_h-C_{80}.

Low-Energy Vibrational Pattern of $Dy_3N@C_{80}$ as Probed by Raman Spectroscopy. The low-energy Raman spectra of $Dy_3N@C_{80}$ are shown for two excitation wavelengths in Figure 6a. Since the energy of the laser wavelength of 647 nm (1.92 eV, lower trace in Figure 6a) matches that of the lowest energetic electronic transitions of $Dy_3N@C_{80}$, a strong resonance Raman enhancement is observed.[6e,7c,7e,23,24] Resonance Raman scattering is also found for the laser wavelength of 514 nm (2.41 eV, upper trace in Figure 5a). Both resonance Raman spectra exhibit an almost identical spectral pattern.

The low-energy Raman spectra of $M_3N@C_{80}$ (I) clusterfullerenes consist in general of radial C_{80} cage modes, which are found at frequencies down to 220 cm^{-1}, and of metal-based modes ranging from 220 to 30 cm^{-1}.[7d,23,24] The latter group includes the in-plane M_3N cluster deformation mode and the frustrated translations and rotations of the M_3N cluster, which are caused by the bond formation between the M_3N and C_{80} fullerene cage.[7d,23,24] These vibrations provide the information on the interaction between the encaged M_3N cluster and the carbon cage, which is an important factor for the stability of the clusterfullerene.[23,24]

In Figure 6b, the low-energy Raman spectra of $Dy_3N@C_{80}$, $Gd_3N@C_{80}$ (I), and $Sc_3N@C_{80}$ (I) obtained with the excitation wavelength of 647 nm are compared. The spectrum of $Dy_3N@C_{80}$ resembles closely that of $Gd_3N@C_{80}$ (I) and is significantly different from that of $Sc_3N@C_{80}$ (I) (see Supporting Information

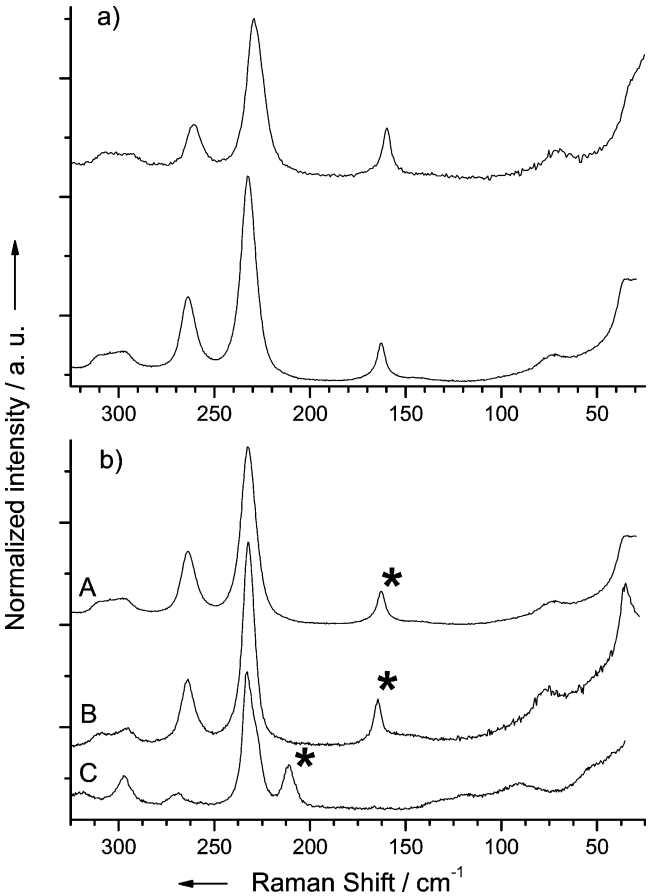

Figure 6. (a) The low-energy Raman spectra of $Dy_3N@C_{80}$ (I) for excitation wavelengths of 514 nm (upper trace) and 647 nm (lower trace). (b) The low-energy Raman spectra of $Dy_3N@C_{80}$ (I) (A), $Gd_3N@C_{80}$ (I) (B), and $Sc_3N@C_{80}$ (I) (C) excited with a 647-nm laser irradiation. The asterisks mark the in-plane M_3N cluster deformation modes.

S2).[7c,23] For instance, the $Dy_3N@C_{80}$ line at 163 cm^{-1} has its $Gd_3N@C_{80}$ (I) counterpart at 165 cm^{-1}, whereas in $Sc_3N@C_{80}$ (I) this mode is up-shifted to 210 cm^{-1} (see Table 1). Likewise, the M_3N-C_{80} vibrational modes, which are correlated to the frustrated translations and rotations of the M_3N cluster, are also found to experience appreciable up-shifts from $Dy_3N@C_{80}$ (74 and 35 cm^{-1}) to $Sc_3N@C_{80}$ (I) (120 and 47.5 cm^{-1}). Because of the significant metal dependence and with the help of DFT vibrational computations performed in this work for $Sc_3N@C_{80}$ (I) and $Y_3N@C_{80}$ (I), strong Raman lines of $Sc_3N@C_{80}$ (I) at 210 cm^{-1}, of $Y_3N@C_{80}$ (I) at 194 cm^{-1}, and of all other $M_3N@C_{80}$ (I) clusterfullerenes at 157−165 cm^{-1} can be assigned to the frustrated in-plane cluster translation partially mixed with the in-plane M_3N deformation. As far as this mode is clearly assigned in the Raman spectra of all $M_3N@C_{80}$ (I) studied to date[7d] and because it is directly related to the cluster−cage bond formation, its frequency may serve as a measure of the strength of the cluster−cage interaction in further analysis.

Table 1 lists the frequencies of this mode for all $M_3N@C_{80}$ (I). The frequencies of the cluster−cage modes are defined by two factors: (1) cluster−cage force constants and (2) mass of the cluster. Hence, meaningful analysis of the cluster−cage interactions on the basis of the vibrational frequencies should distinguish the influence of these two factors as far as the strength of the bond formation is related only to the force constants.[25] Reliable quantum-chemical calculations of the force fields for the clusterfullerenes with rare earth metals are still hardly feasible, while DFT computations for $Sc_3N@C_{80}$ and $Y_3N@C_{80}$ can be easily accomplished. Reliability of the computed force fields for our analysis is confirmed by the good agreement of computed frequencies for the in-plane translational mode of the cluster, 203 cm^{-1} for $Sc_3N@C_{80}$ and 190 cm^{-1} for $Y_3N@C_{80}$, with the experimental values 210 cm^{-1} and 194 cm^{-1}, respectively. Hence, we used the force fields of $Sc_3N@C_{80}$ and $Y_3N@C_{80}$ to simulate the vibrational spectra of other $M_3N@C_{80}$ (M = Gd−Lu) changing the mass of the metals, and two sets of frequencies for the frustrated in-plane translational mode of the cluster were obtained (see Table 1). It appears that the use of $Y_3N@C_{80}$ force field reproduces experimental frequencies for lanthanide-based clusterfullerenes within 5 cm^{-1}, while the frequencies obtained with the use of $Sc_3N@C_{80}$ force field are underestimated by 20−25 cm^{-1}. These numbers clearly show that the cluster−cage interaction is significantly weaker in the case of $Sc_3N@C_{80}$ compared to other $M_3N@C_{80}$ (I). On the contrary, the strength of the cluster−cage interaction in the class II clusterfullerenes is almost the same for all metals. The extent of the cluster−cage interactions does not depend on the symmetry of cluster, which is the same (C_3) for the pyramidal Gd_3N and nearly planar Dy_3N.

The low-frequency range also contains the out-of-plane deformation mode of the cluster, which also shows significant dependence on the cluster composition. In $Sc_3N@C_{80}$ (I), this mode was assigned to the weak far-IR band at 236 cm^{-1}, while it could not be detected in the spectrum of $Y_3N@C_{80}$.[23] In this work, DFT calculations have shown that in $Y_3N@C_{80}$ this mode is considerably softened down to 70 cm^{-1}, and close frequencies may be expected for other class II $M_3N@C_{80}$. Unfortunately, this mode has insignificant Raman and moderate IR intensities, and it is impossible to detect it in the experimental spectra.

Conclusion

We have determined the molecular structure of $Dy_3N@C_{80}$ (I) by an X-ray crystallographic study of single crystal of $Dy_3N@C_{80}$·Ni(OEP)·$2C_6H_6$, revealing a nearly planar Dy_3N cluster encapsulated in an I_h-C_{80} cage. FTIR spectroscopy study of $Dy_3N@C_{80}$ (I) in comparison with other $M_3N@C_{80}$ (I) (M = Sc, Y, Gd, Tb, Ho, Er, Tm) clusterfullerenes revealed the correlation between the antisymmetric M−N stretching vibrations and the structure of M_3N of $M_3N@C_{80}$ (I). Being almost the same for Tm-, Ho-, Er-, and Dy-based $M_3N@C_{80}$ (I), the frequency of this mode becomes considerably lower when the cluster becomes pyramidal in $Gd_3N@C_{80}$ (I). The low-energy Raman pattern of $Dy_3N@C_{80}$ is analyzed to probe the interaction between the encaged Dy_3N cluster and the C_{80} carbon cage. The study revealed that $Dy_3N@C_{80}$ has the similar vibrational structure as well as comparable M_3N-C_{80} interactions to all class II clusterfullerenes $M_3N@C_{80}$ (I), including M = Y, Gd−Lu. On the contrary, cluster−cage interactions in $Sc_3N@C_{80}$ are found to be significantly weaker.

These results lead to the following conclusions: On stepping from $Sc_3N@C_{80}$ (I) to class II $M_3N@C_{80}$ (I) (M = Y, Gd, Tb,

(25) This is contrary to the case of M−N antisymmetric stretching mode, which is defined only by the M−N force constant since displacements of the metal atoms in this vibration are negligible. Hence, $\nu_{as,M-N}$ frequencies of different $M_3N@C_{80}$ (I) can be compared directly.

(26) Kobayashi, K.; Sano, Y.; Nagase, S. *J. Comput. Chem.* **2001**, *22*, 1353−1358.

Dy, Ho, Er, Tm) clusterfullerenes, a significant increase of the ionic radius of the metal first results in an increase of the cluster−cage interaction, which is manifested by softening of the tangential mode frequencies, and the increase of the M_3N-cage force constant, suggesting that the charge transfer from the M_3N cluster to the C_{80} cage becomes stronger. With the further increase of the metal radius in the series of Lu−Gd lanthanide metals, the cluster−cage interactions do not change considerably. At the same time, the strain accumulated by the increase of the ionic radius and corresponding increase of the "cage pressure" results in pushing nitrogen atom out of the M3 plane, that is, pyramidalization of the cluster. This study reveals that Dy_3N is the largest uniform lanthanide metal cluster which remains nearly planar in I_h-C_{80}, while further increase of the ionic radius leads to significant lowering of antisymmetric M−N stretching frequency, pyramidalization of the cluster, and decrease of the yield of the clusterfullerenes. Since this study demonstrates that the cluster size (determined by the ionic radius of the metals involved) plays the dominating role in the structure of the M_3N cluster in $M_3N@C_{80}$ (I), several unknown cluster structures within the lanthanide-based $M_3N@C_{80}$ (I) (M = Tb, Ho, Er, Tm) could be predicted.

Acknowledgment. We thank Mrs. H. Zöller, Ms. K. Leger, and Mr. F. Ziegs cordially for the technical assistance in the fullerene production, HPLC isolation, and spectroscopic characterizations. S. Y. thanks the Alexander von Humboldt (AvH) Foundation for financial support. Financial support from DAAD and CRDF (grant RUC2-2830-MO-06) and computer time at the Research Computing Center of the Moscow State University for A. P. are gratefully acknowledged.

Supporting Information Available: Line shape analysis of the FTIR spectra of $M_3N@C_{80}$ (I) (M = Sc, Y, Gd, Tb, Dy, Ho, Er, Tm), comparison on the low-energy Raman modes of $Dy_3N@C_{80}$ (I), $Gd_3N@C_{80}$ (I), and $Sc_3N@C_{80}$ (I), crystallographic information of $Dy_3N@C_{80}$·Ni(OEP)·$2C_6H_6$ in CIF format. This material is available free of charge via the Internet at http://pubs.acs.org.

JA066814I